$GaAs_{1-x}Bi_x$ Light Emitting Diodes

A New Long Wavelength Semiconductor Light Source

by

Ryan B. Lewis

B.Sc., Dalhousie University, 2006

A THESIS SUBMITTED IN PARTIAL FULFILMENT OF
THE REQUIREMENTS FOR THE DEGREE OF

Master of Applied Science

in

The Faculty of Graduate Studies

(Engineering Physics)

The University Of British Columbia

(Vancouver)

October, 2008

Abstract

$GaAs_{1-x}Bi_x$ is an exciting new semiconductor material, which has been proposed as a new material for infrared light emitting devices. Recent advancements in the growth of $GaAs_{1-x}Bi_x$ films have made it possible to produce $GaAs_{1-x}Bi_x$ light emitting diodes for the first time. Throughout this research we have grown, fabricated and characterized $GaAs_{1-x}Bi_x$ light emitting diodes. Similarly structured $In_xGa_{1-x}As$ light emitting diodes were also produced and characterized for comparison to the $GaAs_{1-x}Bi_x$ devices. Strong electroluminescence was obtained from $GaAs_{1-x}Bi_x$ devices, showing two emission peaks, one corresponding to the $GaAs_{1-x}Bi_x$ layer and the other to the GaAs cladding. Emission from $In_xGa_{1-x}As$ devices was about 100 times brighter than from $GaAs_{1-x}Bi_x$ devices.

Temperature dependent electroluminescence and photoluminescence measurements of a $GaAs_{1-x}Bi_x$ light emitting diode were made and showed some unusual results. The wavelength of the peak in the electroluminescence from the $GaAs_{1-x}Bi_x$ was independent of temperature in the range 100 K to 300 K while the GaAs peak shifted with temperature as expected. Photoluminescence measurements on the same structure show temperature dependence of the peak wavelength similar to the temperature dependence of GaAs.

Table of Contents

List of Tables

List of Figures

Acknowledgements

I would like to thanks my supervisor Tom Tiedje for his inspiration, guidance and for sharing so much of his knowledge and experience with me. Thanks to the rest of the MBE group of being so willing to help me out and for being and so entertaining. Special thanks to Dan Beaton for growing my samples and for helping me with latex, without you this would have been a short thesis.

I'd also like to thank my parents for keeping in such close contact and for providing so much support and encouragement. Thanks to Jeff Dahn at Dalhousie for encouraging me to continue my academic careere in condensed matter physics. And of course thanks to Dayna for putting up with me and cheering me up while I was writing this thesis. Your support has meant so much.

Chapter 1

Introduction

It is hard to imagine a world without semiconductors. These special materials, group IV alloys, III-V alloys, II-VI alloys and recently I-III-VI_2 alloys are an integral part of the technology-driven world that we live in. The III-V class of semiconductors dominate applications for the microwave frequency integrated circuits used in cell phones, light emitting diodes (LEDs), diode lasers for data transmission, reading and recording for DVD and CD players and high efficiency solar cells. III-V's are ideally suited for optical applications because their direct bandgap allows for very efficient generation of light.

GaAs and InP are arguably the most important III-V semiconductors. InP-based lasers are extensively used in fiber optic data transmission. GaAs has a high electron mobility, good for making high frequency transistors, it also has a higher breakdown voltage than silicon, allowing for higher power devices to be made. Despite these advantages, silicon is much more used for integrated circuit manufacturing. Reasons for this are that: silicon is more abundant and easier to process; silicon dioxide, which is one of the best known insulators is easily incorporated into silicon circuits; the higher hole mobility of silicon allows for fabrication of faster p-channel field effect transistors, required for complementary metal-oxide-semiconductor (CMOS)

logic, which makes GaAs-based logic circuits have much higher power consumption. The biggest advantage of GaAs is that it can be easily alloyed with other III-V systems to achieve a wide range of bandgap energies, which allows for easy fabrication of double heterostructures (DH's). DHs are formed by sandwiching a low bandgap semiconductor material between a semiconductor with a higher bandgap. This structure is extremely usefull for optoelectronic devices.

The ability to grow high quality films with energy bandgaps lower than the 1.42 eV GaAs bandgap on GaAs substrates is of much interest for device applications. The silica fibers used for optical data transmission have no dispersion at 1.3 μm and are most transparent at 1.55 μm, which correspond to bandgaps of 0.83 eV and 0.80 eV. The solar cell industry would also like to grow a 1.0 eV material on GaAs for use in high-efficiency multi-junction solar cells, thus much effort has been made in developing such materials. Common bandgap lowering materials used to alloy with GaAs are InAs and GaSb, however because indium is larger than gallium and antimony is larger than arsenic $In_xGa_{1-x}As$ and $GaAs_{1-x}Sb_x$ alloys have a larger lattice constants than pure GaAs. This limits the thickness and compositions that can be grown pseudomorphically on GaAs before the strain causes dislocations to form. Fig. 1.1 shows the energy bandgap as a function of lattice constant for several semiconductor alloys, including the GaAs-InAs and GaAs-GaSb alloys.

The heaviest group III and V elements, thorium and bismuth have been largely neglected as candidates for alloying with GaAs. These elements are difficult to incorporate into the lattice due to their large size and tendency

This figure has been removed due to copyright restrictions. The figure showed a plot of the bandgap of several semiconductor alloys as a function of lattice constant and was obtained from [1].

Figure 1.1: Energy bandgap vs. lattice constant for several semiconductor alloys[1].

to surface segregate[3][4]. First reports of bismuth incorporation into GaAs came from metal-organic vapor phase epitaxy (MOVPE) in 1998 from Oe and Okamoto, who were able to grow $GaAs_{1-x}Bi_x$ with concentrations up to $x = 0.02$[5]. Molecular beam epitaxy (MBE) growth was first presented 5 years later[4][6]. Incorporation of small amounts of bismuth produces a large reduction in the bandgap of GaAs[7]; 88 meV per percent bismuth, which is seven and four times greater than what is achievable with indium or antimony respectively[8] for equal incorporated amounts.

The portion of the periodic table, corresponding to elements found in semiconductors is shown in Fig. 1.3. The red and blue elements can be described as alloying elements with GaAs, while the green elements: nitrogen and bismuth seem to behave more like impurities when incorporated, rather

than forming an alloy. The two ternary alloys GaN_xAs_{1-x} and $GaAs_{1-x}Bi_x$ are complimentary in that GaN_xAs_{1-x} reduces the bandgap by lowering the conduction band minimum (CBM), while $GaAs_{1-x}Bi_x$ lowers the bandgap by raising the valence band maximum (VBM)[8]. In the $GaAs_{1-x}Bi_x$ alloy, the Bi6p level is resonant with the VBM[9], whereas in the case of the GaN_xAs_{1-x} alloy, the N2p levels are deep in the valence band and the unoccupied N2s antibonding orbital is resonant with the CBM[10]. Since nitrogen incorporation decreases the GaAs lattice size and bismuth increases it, the quaternary $GaN_xAs_{1-x}Bi$ alloy has been proposed as strain compensating alloy, allowing low bandgap $GaN_xAs_{1-x}Bi$ to be lattice matched to GaAs[11]. Fig. 1.2 shows the energy bandgap vs. lattice constant for selected III-V semiconductor alloys, including the GaAs-GaN system and the GaAs-GaBi system. The blue line corresponds to the GaAs-GaBi alloy.

Most properties, including bandgap to a first approximation follow Vegard's law[12] when alloying III-V semiconductors, however this is not true for the incorporation of nitrogen. For example, the bandgap of GaN is higher than bandgap of GaAs, however incorporation of small amounts of nitrogen into the GaAs lattice results in a reduction of the GaAs bandgap by the huge amount of 200 meV per percent nitrogen[13][14]. GaBi has not been synthesized, so it's lattice constant and bandgap have only been determined theoretically by density functional theory.

It has been proposed that $GaAs_{1-x}Bi_x$ alloys have an anomalously temperature insensitive bandgap[4]. The temperature dependence of the $GaAs_{1-x}Bi_x$ bandgap has recently been measured, however quite different values were obtained[5][6][15]. Photoluminescence and photoreflectance measurements

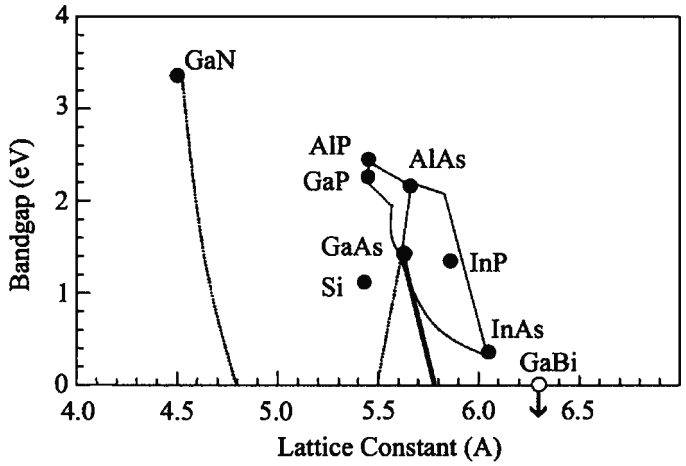

Figure 1.2: Energy bandgap vs. lattice constant for several semiconductor alloys including the GaAs-GaN and GaAs-GaBi systems.

on a sample containing 2.6% bismuth by Yoshida, et al. found the temperature dependence of the $GaAs_{1-x}Bi_x$ bandgap to be 1/3 that of GaAs[5], however other measurements found a similar temperature dependence to GaAs[6].

As the heaviest non-radioactive element, bismuth alloying creates an unusually large spin orbit splitting. Incorporation of bismuth into III/V alloys could provide the large spin-orbit coupling needed for spintronic devices.

The $GaAs_{1-x}Bi_x$ alloy has recently been shown to have very wide photoluminescence (PL) spectra, suggesting the grown films may contain bismuth

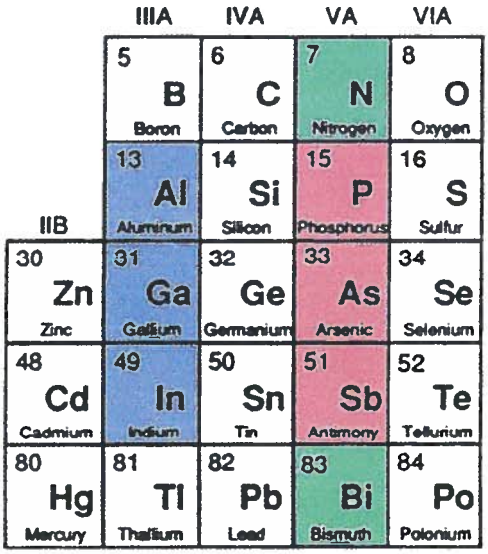

Figure 1.3: The section of the periodic table containing elements used in common semiconductors.

clusters or compositional variations throughout the film. A broad spectrum $GaAs_{1-x}Bi_x$ light emitter could provide the desired light source for optical coherence tomography (OCT)[16][17]. OCT is a medical imaging technique that uses interferometry of low coherence light to image tissue cross sections at depths of a few millimeters, with micron resolution. The resolution of an OCT system is determined by the coherence legnth of the light source used. For a gaussian beam the coherence legnth is given in Eq. 1.1, where λ_o is the central wavelength of the gaussian spectrum, and $\Delta\lambda$ is the full width at half maximum of the spectrum.

$$l_c = \frac{2ln2}{\pi}\frac{\lambda_o^2}{\Delta\lambda} \tag{1.1}$$

For maximum imaging depth the light source must operate in the near infrared range ($850 - 1300$ nm) where tissue is most transparent. These demands perfectly overlap with the characteristics of the $GaAs_{1-x}Bi_x$ alloy, thus OCT is a very promising application of a $GaAs_{1-x}Bi_x$ light emitters.

Throughout this research we have fabricated and characterized $GaAs_{1-x}Bi_x$ light emitting diodes. To our knowledge, these results represent the first $GaAs_{1-x}Bi_x$ LEDs ever made. We discuss in detail the growth and fabrication processes that we have developed. Current-Voltage, temperature dependent photoluminescence and electroluminescence results are also presented and discussed for this exciting new semiconductor.

Chapter 2

Growth and Properties of the $GaAs_{1-x}Bi_x$ Alloy

2.1 Molecular Beam Epitaxy Growth of GaAs Alloys

Gallium Arsenide is probably the most important material for solid state light emitting devices. GaAs is advantageous because of it's high electron mobility, ease of manufacturing, availability of 150 mm wafers and ability to be alloyed with other elements to modify the GaAs bandgap. GaAs, as many III-V semiconductors has a direct bandgap, allowing for much more efficient optical devices to be made, compared to elemental semiconductors like silicon and germanium. The direct bandgap means transitions between the conduction band minimum (CBM) and valance band maximum (VBM) can occur without either the absorption or emission of phonons, to conserve momentum.

Molecular beam epitaxy (MBE) is a common method for the preparation of GaAs based semiconductor materials in thin film form. MBE is a process, where beams of atoms or molecules (usually from thermal evaporation) are

simultaneously incident on a heated substrate in ultra-high vacuum (UHV). Individual beams can be turned off or on in a fraction of a second by the use of shutters. This process allows for precise control of compositions and layer thicknesses on the sub-monolayer scale and the ability to abruptly change the composition of the layer being grown. Typically, GaAs is grown at rates of about 1 μm per hour at temperatures of about half the melting point of GaAs or 500°C to 650°C. The fact that growth takes place so much colder than the melting point allows for metastable compounds, not found in nature to be created. Low temperature also minimizes the number of thermodynamic defects in the grown material.

2.2 Growth of the $GaAs_{1-x}Bi_x$ Alloy

Under normal GaAs growth conditions, bismuth tends to surface segregate and does not incorporate into the GaAs lattice. At these conditions bismuth behaves as an ideal surfactant, as it does not incorporate. Bismuth has been used as a surfactant in the growth of several GaAs-based material systems, such as GaAs and $In_xGa_{1-x}As$ where it has been shown to improve surface smoothness and photoluminescence [18][19][?]. In the case of GaN_xAs_{1-x} and $InGaN_xAs_{1-x}$ it has been shown to result in smoother surfaces, enhanced nitrogen incorporation, and increases photoluminescence by reducing defects [3][19].

Incorporation of bismuth into the GaAs lattice requires atypical growth condidions, to reduce the tendency of bismuth to surface segregate and reduce the competition for group V sites. To achieve this, low growth temper-

atures and low V:III ratios (usually 1:1 to 4:1 compared to typical ratios of about 10:1) are required. High bismuth incorporation of up to 10% has been achieved in the temperature range of 270°C-320°C[1]. Low growth rates of about (1 nm/min) are used in order to have more control over the excess bismuth on the surface and minimize the likelihood of bismuth accumulation in the form of droplets[1]. Droplets are very undersirable as they lead to local variations in the amount of bismuth coverage and hence the local composition. Droplets also increase the surface roughness. In the case of low growth rates, the rate of bismuth incorporation is less, so lower bismuth fluxes can be used. In this case most of the incident bismuth flux is evaporated, rather than incorporated, thus allowing for more control over the amount of surface bismuth present. Low temperature growth also leads to a larger critical thickness before dislocations form[1], which allows for high strain, small bandgap, epi-layers to be grown on GaAs without relaxation.

Fig. 2.1 shows [004] X-ray rocking curves for three $GaAs_{1-x}Bi_x$ epilayers for x values of 1.4%, 5% and 10%[1]. Fits to each data set are shown as dotted lines. The sharp peak in each spectra corresponds to the [004] GaAs substrate peak and the smaller satelite peak on the left corresponds to the $GaAs_{1-x}Bi_x$ epilayer. Dampled pendellosung fringes are visible in all the curves, indicating high structural quality. These interference fringes also allow for determination of layer thicknesses. Composition is determined from the separation in epilayer and substrate peaks using the known shift of 300 arcsec per percent bismuth incorporation in the [004] X-ray peak for incorporation up to a few percent. The shift in lattice constant with bismuth has been determined by comparing Rutherford backscattering (RBS) compo-

sitional data to X-ray diffraction data on samples with up to 3.1% bismuth by Tixier et al.[3]. Since the lattice constant of zincblend GaBi is unknown, one could not use Vegard's law to determine composition from X-ray data alone, however the work by Tixier et al. has provided a theoretical prediction of the GaBi lattice constant of 0.6336 nm based on an extrapolation of concentrations up to 3.1%[3]. Thus bismuth compositions can now be determined by X-ray diffraction, in comparison to this work.

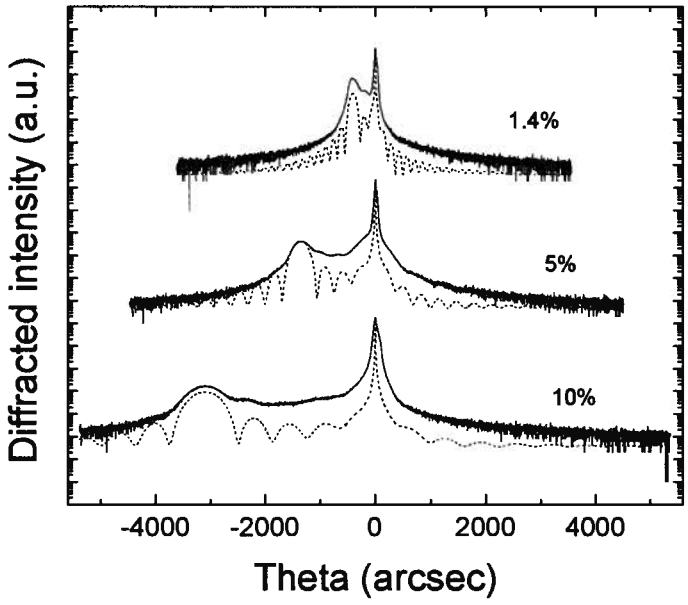

Figure 2.1: [004] X-ray rocking curves for three $GaAs_{1-x}Bi_x$ epilayers. A fit to each curve is shown with dotted lines[1].

2.3 Doping and the p-n Junction Diode

In the case of a semiconductor, the covalent bonding results in heavy overlap of the atomic wavefunctions between neighboring atoms. When two atoms are covalently bonded together their atomic energy levels split to produce two energy states, the lower energy state is called the bonding state and the upper the antibonding state. For n atoms covalently bonded this splitting produces n energy levels, which, for large crystals form energy bands [20]. The electronic energy level distribution can be found by solving the Schroedinger equation for a periodic potential, corresponding to the appropriate atomic potentials. At zero temperature, the electrons of the crystal populate the energy states by filling up levels from lowest to highest. The highest filled energy band is called the valence band and the lowest unoccupied band is called the conduction band. Direct bandgap semiconductors are semiconductors where the valence band maximum (VBM) and conduction band minimum (CBM) occur at the same value of electron momentum. Compound semiconductors, such as GaAs, InSb and GaN are direct bandgap semiconductors. Silicon, germanium and AlAs are examples of indirect bandgap semiconductors, which have an offset in momentum between the CBM and VBM. A direct bandgap is required for efficient light generation as photons are created by downward transitions from the conduction band to the valence. Transitions in indirect bandgap semiconductors usually involves the creation or destruction of phonons in addition to photons.

A pure semiconductor at zero temperature has all energy states in the valence band occupied and all conduction band states vacant. The energy at which there is a 50 percent probability that the state is occupied is called

the Fermi energy. The occupation of energy states as a function of energy is given by the Fermi function, given in Eq. 2.1, where E_f is the Fermi energy.

$$f = \frac{1}{e^{(E_1 - E_f)/kT} + 1} \tag{2.1}$$

The Fermi energy for an intrinsic semiconductor is close to mid-gap. The addition of small amounts of impurity, as low as 1 ppb can greatly shift the Fermi energy, because there are no allowed energy levels between the bands. Donor dopants are impurity atoms that have occupied energy levels close to the conduction band minimum, which shift the Fermi level towards the conduction band, resulting in an n-doped material. At non-zero temperatures, electrons can be excited from the donor atom into the conduction band, populating the conduction band. Similarly, acceptor impurities are atoms that have unoccupied levels near the valence band maximum, which shift the Fermi level down, towards the valence band, resulting in a p-doped material. These levels can accept electrons from the valance band.

In the case of a p-n junction, p and n-doped materials are put in intimate contact with each other. At equilibrium (under no electrical bias) the Fermi energy must be equal throughout both materials. This causes band bending near the junction, a result of the redistribution of charge in the region close to the junction, known as the depletion region. This redistribution of charge causes a built in voltage to be produced, which equals the initial difference in Fermi energies of the two materials. Fig. 2.2 shows a schematic drawing of the valance and conduction band energies of a p-n junction at equilibrium.

Applying a forward bias causes a flattening of the bands and a shrinking of the width of the depletion region. Biasing the diode results in a non-

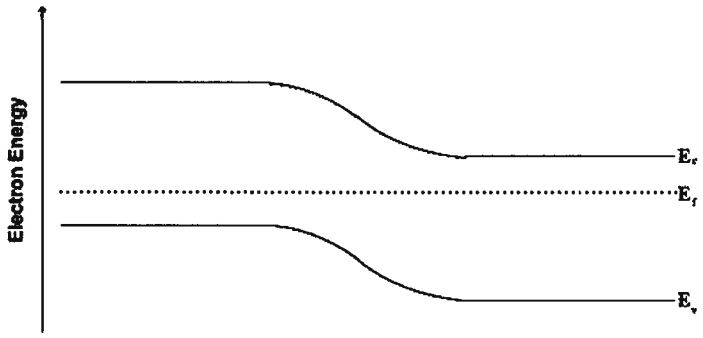

Figure 2.2: Schematic diagram p-n junction at equilibrium (no applied bias).

equilibrium condition and produces two separate quasi-Fermi levels, one on each side of the junction [21]. Fig. 2.3 shows a hypothetical p-n junction under forward bias. The figure shows an area near the junction, where conduction electrons and holes exist together in the same space, allowing recombination to take place and light to be created. Under high enough forward bias voltages it's possible to create a population inversion at the junction making it possible for lasing to take place.

The diode current, I of an ideal diode with an applied voltage V_d is given by the diode equation shown in Eq. 2.2 where I_s is the saturation current, n is the ideality factor of the diode and V_T is the thermal voltage. The thermal voltage is given in Eq. 2.3, where k is the Boltzmann constant, T is the temperature in Kelvin and e is the electron charge. The ideality factor of diodes usually ranges between 1 and 2, depending on the type of diode. For devices where recombination in the depletion region is negligible, i.e electrons and holes can be assumed to slip through the depletion region without recombining, the theoretical ideality factor is 1. In this case electrons

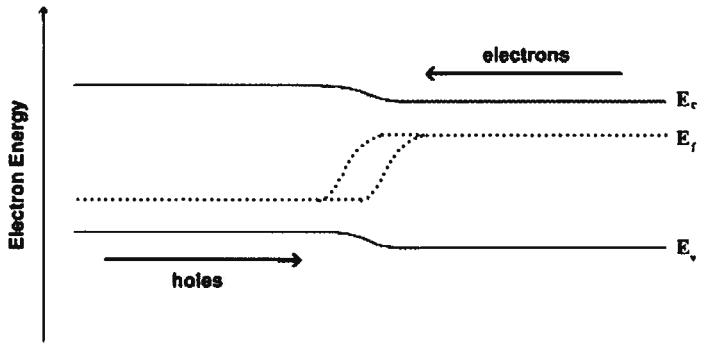

Figure 2.3: Schematic diagram of a forward biased p-n junction.

are injected directly into the p-region and holes into the n-region. In the case of an LED double heterostructure (DH), ideally all the injected carriers will recombine in the depletion region radiatively [20] and thus the ideality factor would be 2. This is the case because carriers only have to travel half way across the built in potential before recombining. In many practical cases the recombination in the depletion region can be dominated by non-radiative recombination.

$$I = I_s(e^{V_d/nV_T} - 1) \tag{2.2}$$

$$V_T = \frac{kT}{e} \tag{2.3}$$

2.4 Heterostructure Design

Modern LEDs and laser diodes typically can have an array of complicated structures, to improve confinement and overlap of the carriers and photons

and to increase light output. Low index (high bandgap) $Al_xGa_{1-x}As$ cladding layers are used to increase carrier confinement. The active region of these efficient light emitting devices typically consists of multiple low bandgap quantum wells (QWs) spaced with a GaAs layers and this region is typically sandwiched between $Al_xGa_{1-x}As$ cladding layers. Typical thicknesses of the undoped active region containing the QWs is 100 nm to 200 nm[20]. The simplest DH structure that one can imagine in one where there is simply one low bandgap QW layer inside the undoped active region and there is no $Al_xGa_{1-x}As$ cladding. Such a device is relatively simple to make and does not require as much optimization as a more complicated structure. Such a structure was used in making the $GaAs_{1-x}Bi_x$ LEDs in our lab because of the relative difficulty in growing $GaAs_{1-x}Bi_x$ layers. In growing $In_xGa_{1-x}As$ LEDs a similar structure was adopted, but instead of one QW, the active region contained three $In_xGa_{1-x}As$ QWs.

2.5 Light Emitting Diode Growth and Characterization

LED samples were grown in a VG-V80H molecular beam epitaxy (MBE) system on [100] GaAs substrates using effusion cells for gallium, bismuth and indium, a dual stage cracker for As_2, along with a gas injection system for CBr_4 for p-type doping. n-type doping was achieved using a Si effusion cell for samples r1962 and later, and a $SiBr_4$ gas injection system for earlier samples . The substrate temperature was monitored throughout the growth process by optical bandgap thermometry[22] with an accuracy of 5°C. Beam

equivalent pressures were measured using a retractable ion gauge. Growth conditions for GaAs were: V:III ratios of 8:1; growth rate approximately 1 μm/hr; arsenic cell temperature 400°C; gallium cell temperature 950°C; and substrate temperatures between 550°C and 580°C in most cases.

The active region of the bismuth LED n-i-p structure (r1965) consisted of a 30 nm $GaAs_{1-x}Bi_x$ layer sandwiched between two 25 nm undoped GaAs spacer layers. Thicknesses may have varied for different samples. The diodes were grown on n-doped (2×10^{18} cm^{-3}) [100] GaAs substrates (with exception of sample r1810 grown on p-type substrate). A 1000 nm n-doped buffer was grown first at standard GaAs growth conditions with a doping concentration of 5×10^{17} cm^{-3}. The growth was often interrupted between the n-doped layer and the undoped layer to adjust growth conditions as follows: new substrate temperature of 300°C, arsenic cell temperature of 350°C and gallium cell temperature of 850°C for r1965. The temperature of the Ga cell was lowered to achieve a growth rate of 0.1 μm/hr and the arsenic cell temperature was lowered to allow for better control over the As_2 flux at low group V over pressure. Growth interruptions lasted for 10 minutes and were necessary for growths using the $SiBr_4$ since using $SiBr_4$ required additional time in the i-region to switch to the CBr_4. This delay was for the gas lines to be pumped free of the $SiBr_4$ before they could be filled with CBr_4 for p-doping could start. The addition of the elemental silicon effusion cell allowed future growths to avoid this growth interrupt. Samples r1970 and later did not have growth interrupts. Some early LED growth attempts had an additional growth interrupt at the i to p interface as well (r1917 and r1930). The undoped region was comprised of 30 nm of $GaAs_{1-x}Bi_x$ with

25 nm of GaAs on either side. This entire region was grown at low growth rate (0.1 μm/h). The two surrounding GaAs regions were grown at standard As_2 overpressure, while the $GaAs_{1-x}Bi_x$ layer was grown with the As_2 overpressure lowered to nearly stoichiometric levels (2.5:1 for r1965) to enhance bismuth incorporation. Bismuth flux was present at the substrate for the entirety of the intrinsic region, as bismuth will not incorporate until the As_2 flux is lowered, even at low substrate temperatures. No growth interruption was used for the transition from intrinsic to p-doped layers in most cases. The growth rate and substrate temperature were ramped back to standard conditions while still growing, causing a small region (25 nm) where the p-doping was non-uniform in the case of no second growth interrupt. 1000 nm of p-doped (5×10^{17} cm^{-3}) GaAs was grown followed by 100 nm of highly p-doped (approximately 5×10^{18} cm^{-3}) GaAs. The highly doped capping layer was used so that ohmic contacts could be more easily achieved, although higher doping in the 10^{19}/cm^3 range would have been preferred.

Layer thicknesses and compositions were measured by high resolution X-ray diffraction (XRD) using a Philips Xpert diffractometer. Rocking curves were measured for the [004] GaAs diffraction peak over ranges of 2^o and 4^o. Fig. 2.4 shows a [004] rocking curve for the most luminescent $GaAs_{1-x}Bi_x$ LED (r1965). The red curve in the figure corresponds to a fit to the data using Bede RADS Mercury, which models diffraction patterns using the dynamical theory of diffraction. The fit shown corresponds to a 30nm $GaAs_{1-x}Bi_x$ layer with $x = 0.018 \pm 0.004$. The split off peak from the $GaAs_{1-x}Bi_x$ layer had low intensity (compared to similar $GaAs_{1-x}Bi_x$ epilayers) due to it being buried under about 1μm of GaAs. This effect combined with the peak not being fully

separated from the GaAs substrate peak resulted in the large uncertainty in the $GaAs_{1-x}Bi_x$ composition. Small pendellosung fringes can be seen in the data, which correspond to reflections from the top GaAs-layer-$GaAs_{1-x}Bi_x$-layer interface. Fitting these fringes we find that the thickness of the top layer is 890 nm. Two other $GaAs_{1-x}Bi_x$ n-i-p structures, one containing about 0.9% Bi and the other 5.5% Bi are shown in Fig. 2.5. Table 2.1 summarizes all the LED structures that were grown.

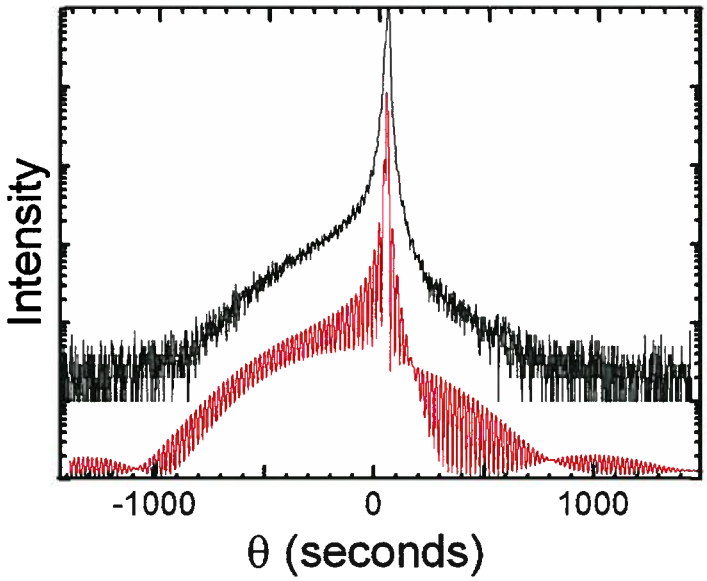

Figure 2.4: [004] rocking curve of a $GaAs_{1-x}Bi_x$ LED sample (r1965) containing 1.8% bismuth. A fit to the data is shown in red

$In_xGa_{1-x}As$ LEDs were grown for comparison with the $GaAs_{1-x}Bi_x$ LEDs. The n-type and p-type layers of these devices were similar to the structure discussed above, however the intrinsic region contained either a single

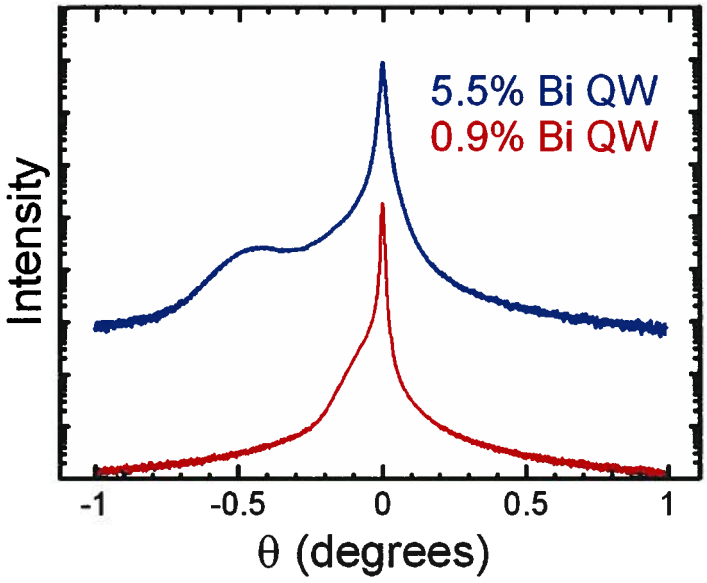

Figure 2.5: [004] rocking curves for two $GaAs_{1-x}Bi_x$ LED samples (r1895 and r1917) containing 0.9% and 5.5% bismuth shown in red and blue.

$In_xGa_{1-x}As$ QW in r1810 or 3 $In_xGa_{1-x}As$ QWs in r1929. r1810 had no growth interrupts while r1929 had one interrupt at the n-i interface. For r1929 $x = 0.18$, each QW was about 5 nm thick, spaced by about 19 nm of GaAs, resulting in an intrinsic region thickness of about 90 nm. Thicknesses are approximate because a good fit to the data could not be obtained. The XRD pattern is shown in Fig. 2.6. The figure contains a fit to the data, which does line up with all the peaks in the curve, but does not correctly model the relative heights. The discrepancies between the XRD data likely comes from small differences in the thicknesses and compositions of the layers, which were not account for because a supercell model was used. The composition

of the QWs was obtained by electroluminescence (EL), discussed in chapter 4. The intrinsic region of r1929 was grown with Ga and In cell temperatures of 950°C and 800°C, respectively at a growth rate of about 1 μm/hour. The substrate temperature was 580°C and there was a growth interrupt at the p-type to intrinsic interface. At the time of this growth n-doping was done with gas source $SiBr_4$, so the growth interrupt was necessary to pump out the gas lines (as discussed above). The growth interrupt lasted 8.5 min.

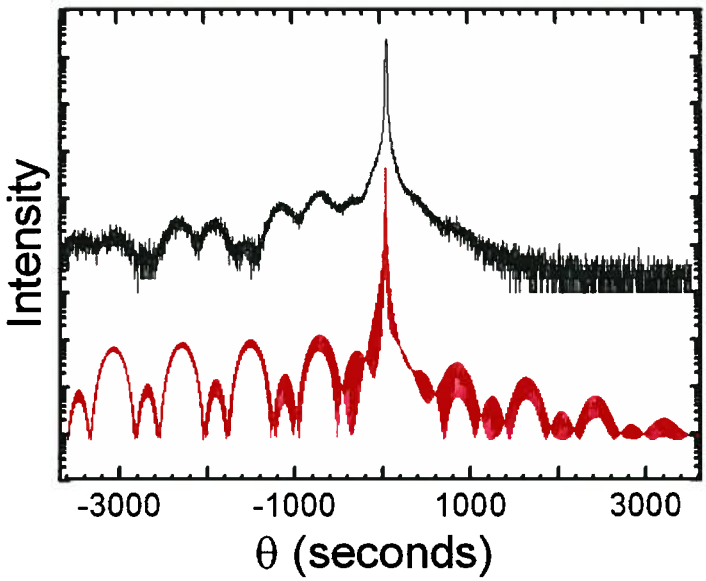

Figure 2.6: [004] rocking curve of a $In_xGa_{1-x}As$ LED sample (r1929) containing 18% indium. A fit to the data is shown in red

Table 2.1 summarizes LED growths and characteristics of all grown samples. Many samples contain little or no bismuth and were not fabricated into LED's. Getting bismuth to incorporate proved to be very difficult. The

conditions for bismuth incorporation are very precise and perhaps if detailed calibrations of fluxes were done before each growth then more reproducible compositions of $GaAs_{1-x}Bi_x$ layers would have been obtained. Table 2.2 gives more detailed growth information from the most significant samples. Beam equivalent pressures (BEPs) are given as read from ion gauge and are based on flux calibrations done weeks or even months before the actual growths. BEPs have not been corrected for the sensitivities of different chemical species.

Table 2.1: Summary of all light emitting diode samples grown, including failed attempts.

Sample Log #	Growth Interrupts	Bi or In [%]	EL	Wavelength (nm)	Comments
r1810	0	In[3.6]	medium	900	very resistive
r1852	0	In[0]	NA	NA	did not rectify
r1875	0	In[21]	NA	NA	very leakey, over doped p-layer
r1888	1	Bi[0.5]	NA	NA	not tested, wanted more Bi
r1895	1	Bi[0.9]	None	NA	only defect emission
r1901	1	Bi[0]	NA	NA	not tested, no Bi
r1917	2	Bi[5.5]	Very weak	1300	mostly defect emission and GaAs
r1929	1	Inx3[18]	Strong	1025	very strong EL, good IV
r1930	2	Bi[NA]	NA	NA	dropped in MBE-post growth
r1962	1	Bi[NA]	NA	NA	covered in Ga during growth
r1965	1	Bi[1.8]	Strong	986	see text
r1970	0	Bi[0]	NA	NA	not yet tested
r1982	1	GaAs	NA	NA	high T GaAs not yet tested
r1985	0	Bi[0]	NA	NA	not yet tested

Table 2.2: Summary of growth conditions of significant samples.

Sample Log #	Substrate Temp. (°C)	P[Ga] (torr)	P[As] (torr)	P[In or Bi] (torr)
r1895	315	3.0×10^{-7}	2.9×10^{-7}	[Bi]3×10^{-9}
r1917	305	1.8×10^{-7}	1.6×10^{-7}	[Bi]6×10^{-9}
r1929	580	9.4×10^{-7}	4.9×10^{-6}	[In]3×10^{-7}
r1965	310	0.8×10^{-7}	0.7×10^{-7}	[Bi]7×10^{-9}

Chapter 3

Post-Growth Fabrication of Light Emitting Diodes

3.1 Ohmic Contacts

One challenge faced in post-growth fabrication of semiconductor electrical devices is making reliable ohmic contacts. An ohmic contact is an electrical contact, which has a linear I-V responce curve, and ideally should have the lowest series resistance possible. Contacts should be easily reproducible and stable over the usable temperature range of the device. This seemingly simple task has been the focus of an enormous amount of research over the past several decades. For more information and selected review articles on ohmic contacts Modern GaAs Processing Methods by Williams [23] contains much useful information, also see the review article by Shen[24] .

Normally, when a metal is put in intimate contact with a semiconductor, a depletion region forms in the semiconductor, which bends the bands so that the Fermi level is equal in the metal and the semiconductor. One would expect that the voltage across the barrier (ϕ_b) would simply be the difference in the work function of the metal (ϕ_m) and the electron affinity (χ) for the case of an n-type semiconductor as shown in Eq. 3.1. In the case of a p-type

semiconductor, it would be expected that the barrier voltage would be the difference between the ϕ_m and the sum of χ and the bandgap energy (E_g), as shown in Eq. 3.2 and illustrated in Fig. 3.1. Fig. 3.1 shows a schematic of band bending for an ideal metal to n-type semiconductor interface as described above.

$$\phi_{b-n\ type} = \phi_m - \chi \tag{3.1}$$

$$\phi_{b-p\ type} = \phi_m - (\chi + E_g) \tag{3.2}$$

Based on this reasoning, by choosing metals with different work functions it should be possible to achieve a large range of values for ϕ_b. A metal-semiconductor combination where $\phi_b = 0$ should result in an ohmic contact, based on this logic. In practice, most metals have the same barrier height of about 0.8 V when put in contact with n-doped GaAs, even though the above discussion would predict that barrier heights from 0.07 V to 0.57 V should be possible [23]. The reason is that the surface states of the semiconductor actually set the barrier height. Fig. 3.2 shows a schematic of a more realistic metal to n-type semiconductor interface.

Current can flow across the metal-semiconductor interface by either thermionic emission, or quantum mechanical tunneling through the barrier, which can be enhanced by applying a large electric field (field emission). Thermionic emission is the main mechanism for current flow through a Shottky diode, while current flow through ohmic contacts is usually due to tunneling. The current density for field emission through a barrier of height ϕ_b has the form of Eq. 3.3, where e is the magnitude of the electron charge and E_{oo} is given

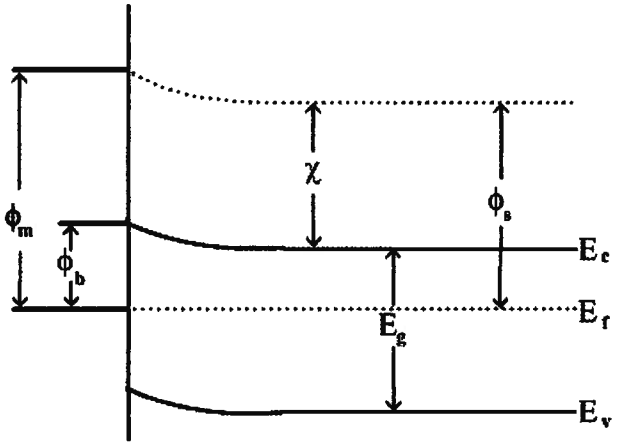

Figure 3.1: Schematic diagram of a metal to n-type semiconductor interface in the absence of surface states.

in Eq. 3.4. Here $\hbar$ is Plancks constant, N is the doping concentration, ϵ is the dielectric constant and m* is the effective mass[25]. It is worth noting that as the doping is increased the tunneling current increases exponentially. This is attributed to narrowing of the depletion region/barrier.

$$J \; \alpha \; exp^{-e\phi_b/E_{oo}} \tag{3.3}$$

where

$$E_{oo} = \frac{e\hbar}{2}\sqrt{\frac{N}{\epsilon}} \tag{3.4}$$

To make a good ohmic contact it's necessary for the surface layer to be highly doped (usually in the 10^{19}cm^{-3} range for n-type and 10^{20}cm^{-3}) range for p-type[23]. To achieve this high level of doping the contact ma-

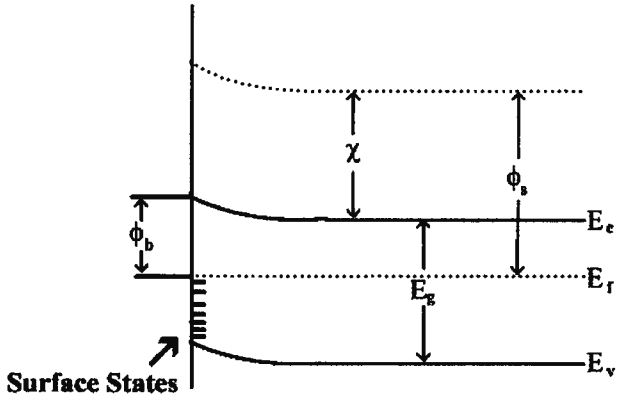

Figure 3.2: Schematic diagram of a metal to n-type semiconductor interface with surface states.

terial usually contains an element, which will diffuse upon annealing into the semiconductor, producing a highly doped surface layer. In the case of AuGe n-contacts, which were used for n-type contacts here, this element is germanium[23]. For contacting n-type GaAs, AuGe-based contacts have been the most successful, even though they are somewhat inconsistent and the resistivity depends strongly on how well optimized the annealing conditions are. Typical contact resistivities of AuGe-based contacts range from 0.8×10^{-6} Ωcm^2 to 4×10^{-6} Ωcm^2[23].

Another method for improving ohmic contacts is to grade the composition of the surface layer by alloying, into a low bandgap semiconductor, such as InAs. This method is not widely used for GaAs as many complications, such as lattice matching arise[23].

Many different material combinations are used to make ohmic contacts to GaAs. For contacting the p-doped side of our LED's Ti/Pt/Au contacts were

used[26][27]. These contacts were selected because of their stability over a the wide annealing range of 420 C to 530 C and extremely low demonstrated contact resistance of 2.8×10^{-8} Ωcm^2[26]. Small circular Ti/Pt/Au p-type ohmic contacts with a diameter of 0.32 mm were deposited through a metal shadow mask using e-beam evaporation. Ti/Pt/Au thicknesses of about 50 nm/100 nm/200 nm were used. Each circular p-type contact defined a single device on top of the wafer. n-type contacts were made by evaporation of Ni/AuGe/Au [23][28] onto the entire back side of the sample, forming a common contact with all the top contacts on the sample. Ni/AuGe/Au thicknesses of about 25 nm/100 nm/200 nm were used. Proper annealing temperatures for the n-type contact on the back were ignored because of the large surface of the contact. After deposition, the wafer was annealed at 450°C for 20 seconds after deposition to improve the contact conductivity.

The resistivity of Ti/Pt/Au contacts was tested by depositing a line of the 0.32 mm diameter metal dots onto an p-doped (about 2×10^{18} cm^{-3}) GaAs wafer cleaved to be about 1 mm by 25 mm. Contact resistances of about one ohm were found by measuring the resistance between dots as a function of separation distance, corresponding to a specific resistivity of about 5×10^{-4} Ωcm^2. It is expected that much lower contact resistivities could be obtained if higher doping concentrations were used, but these values were deemed adequate for test LEDs. Current voltage curves were confirmed to be linear over the current range of interest and dot-to-dot uniformity was excellent.

3.2 Mesa Etching

After contacts were deposited and annealed, the top 300 nm of highly doped GaAs around the contacts was etched off using a H_2SO_4:H_2O_2:H_2O wet etch with volume ratios of 4:1:5[23], which removed 5μm/min for a room temperature solution. The highly doped top layer was removed to minimize current spreading. This etch was selected because it did not seem to damage the Ti/Pt/Au contacts, while some other etches removed the metal all together. The depth of the etch was measured with profilometry. It was discovered that etching through the intrinsic region resulted in high leakage and no light emission, attributed to non-radiative surface recombination. After mesas were etched, the sample was cleaved into sizes of about 5 mm by 3 mm and bonded to a small piece of copper using silver epoxy. Contact was made to the dots by wire bonding the dots to terminals, which were glued to the copper piece. Fig. 3.3 shows a schematic of the LED chip after metalization and etching. The dashed lines indicate possible growth interrupts (depending on the sample). Most early samples were not etched, resulting in poor current-voltage characteristics.

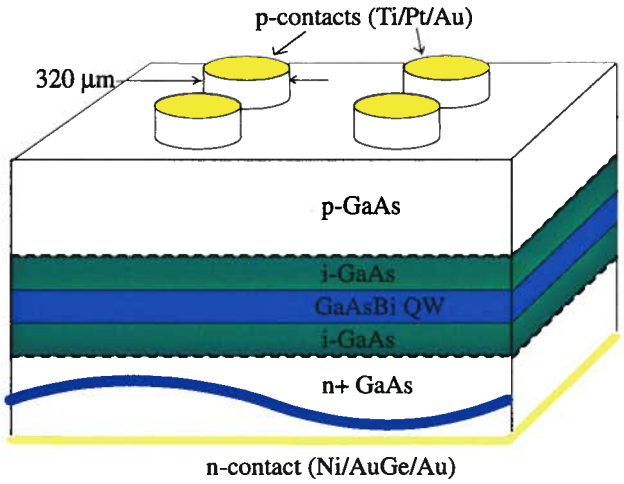

Figure 3.3: Schematic of an LED chip after metalization and etching. Typical thickness for i-GaAs layers was 25 nm, typical GaAsBi QW thicknesses were 30 nm to 50 nm and typical p-GaAs thickness was 1 /mum. The top 300 nm of the p-GaAs layer was removed by etching.

Chapter 4

Electrical Characterization

4.1 Current-Voltage Measurements of $GaAs_{1-x}Bi_x$ Diodes

Current-Voltage (I-V) measurements were made with a Keithley 220 current source and a Keithley 197A voltmeter, using a 2-probe method. According to Keithley specification sheets the current source had an output resistance greater than 10^{14} Ω, absolute accuracy of sourced currents less than 0.1% over the current ranges used and 100 ppm noise in the source. The voltmeter had a resistance greater than 1 GΩ in the 2 V range and a resolution of 10 μV. Both the current source and voltmeter were interfaced to a computer through an IEEE 488 interface, and controlled using an in-house-made LabView program. I-V measurements were made over the current ranges from 10 μA reverse bias to 10 mA forward bias, usually with 10 data points taken per decade and a minimum step size of 100 nA. Unless otherwise mentioned, I-V measurements were made at room temperature.

Fig. 4.1 shows current-voltage measurements of several devices from sample r1965, containing 1.8% bismuth. r1965 was the only $GaAs_{1-x}Bi_x$ LED to show strong electroluminescence and it thus highlighted here. Dot to dot uniformity was excellent, as the curves have excellent overlap.

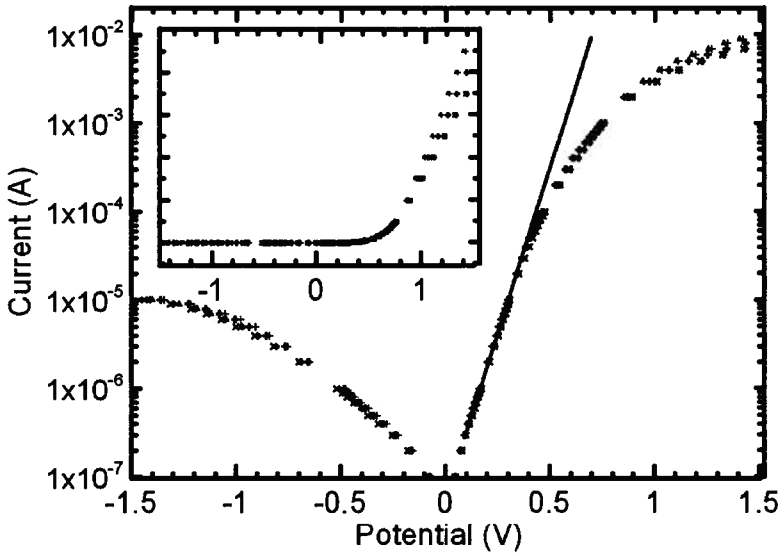

Figure 4.1: Current-Voltage curves for four $GaAs_{1-x}Bi_x$ light emitting diodes at 300 K. The red line indicates a fit to the data with $n = 2.26$ ideality factor.

The leakage current was approximately 5 μA at a reverse bias of 1 V. Fitting the forward bias data over the current range 10^{-7} A to 10^{-5} A to the diode equation gives a saturation current (I_o) of 7.1 $\mu A/cm^2$ with a standard deviation of 0.4 μA between dots. The fit also gave ideality factor of 2.26. Series resistances of 100 Ω with standard deviation of less than 10 Ω were measured at high currents. The reason for the high series resistance is unknown. The resistance is believed not to be due to the ohmic contacts, as contact resistance is expected to be less than 1 Ω as inferred from measurements on the p-doped wafer, which had similar doping concentrations.

Fig. 4.2 shows current voltage data for another $GaAs_{1-x}Bi_x$ sample (r1895), which was found to emit some light. The hollow data points with low reverse bias leakage current are from different diodes for a device prepared soon after growth, where no etching was done to remove the top highly doped GaAs layer. The sample was remeasured after about 2 months (red solid circles) and reverse bias leakage was an order of magnitude greater. The sample was then dipped in HCl to remove any oxide that may have formed and remeasured (black solid diamonds), where it showed the same level of high leakage. A second sample was fabricated from growth r1985, where the top highly doped GaAs layer was removed, but still showed the high leakage (pink solid triangles) observed before. This very unusual degradation has no obvious explanation.

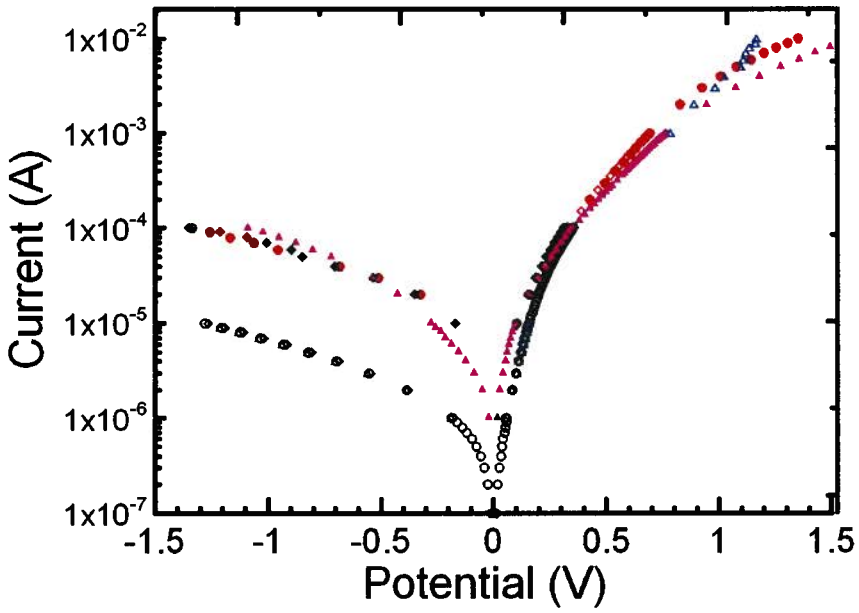

Figure 4.2: Current-Voltage curves for $GaAs_{1-x}Bi_x$ LED r1895. Hollow data points (low leakage values on reverse bias) correspond to dots from an un-etched device fabricated soon after growth. Solid data points (high leakage) correspond to measurements made on the same sample 2 months later, with and without dipping the sample in HCl to remove possible oxide and also for a new device fabricated from the wafer with etched mesas (solid pink triangles).

4.2 Current-Voltage Measurements of $In_xGa_{1-x}As$ Diodes

Fig. 4.3 shows I-V curves for three $In_{0.18}Ga_{0.82}As$ diodes fabricated from sample r1929 at the same time. The top highly doped layer of GaAs was removed by etching. The leakage current at -1 V was observed to be about 0.5 μA (an order of magnitude less than for the $GaAs_{1-x}Bi_x$ sample r1965). Dot to dot uniformity was very good on reverse bias and for forward bias for voltages less than 0.4 V. At higher voltages the diodes behaved very inconsistently. Only the red curve in Fig. 4.3 showed the expected "rolling over" on the semilog plot due to the series resistance dominating the I-V shape, the red and black curves appeared to roll over at 0.5 V, but then curved back up before rolling over again. One possible explanation for this is that irreversible changes were taking place in these samples causing the devices to fail. The diodes were only tested once so this explanation has not been confirmed. All the diodes were observed to be strong light emitters.

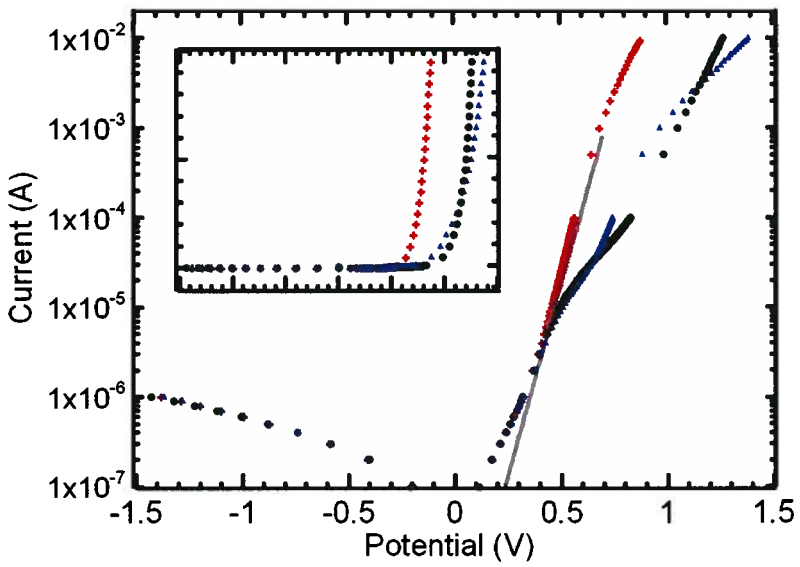

Figure 4.3: Current-Voltage curves for $In_xGa_{1-x}As$ LEDs from sample r1929.

Chapter 5

Optical Characterization

5.1 Electroluminescence (EL) and Photoluminescence (PL)

Luminescence is the emission of photons of light when an atom, molecule, or crystal system decays from an excited state to a lower energy state. Types of luminescence are classified by the method of excitation. Here we discuss electroluminescence (EL), which is the emission of photons, by a material in responce to an applied voltage. We also discuss Photoluminescence (PL), which is the absorption and then re-emission of photons by a material.

Electrons can transition from an occupied initial state to a vacant final state, where the occupation probability of an energy state is given by the value of the Fermi function. The absorption and stimulated emission rates R_{12} and R_{21} and the spontaneous emission rate R_{sp} thus can be written in the form in Eq.5.1, where R_r and R_o are the transition rates of stimulated and spontaneous processes if all state pairs are available. f_v and f_c are the Fermi functions for the valence and conduction bands. Using Einsteins coefficients A and B as rate constants for spontaneous and stimulated processes respectively $R_o = A$ and $R_r = BW(\nu)$, where $W(\nu)$ is the radiation spectral density[20].

$$R_{12} = R_r f_v(1 - f_c) \tag{5.1}$$

$$R_{21} = R_r f_c(1 - f_v) \tag{5.2}$$

$$R_{sp} = R_o f_c(1 - f_v) \tag{5.3}$$

In the case of PL in semiconductors, light with energy greater than the bandgap is incident on the semiconductor. Electrons in the valence band absorb photons and are excited to the conduction band, creating electron hole pairs, which can recombine either radiatively, or by a non-radiative process. The main types of non-radiative recombination processes in semiconductors are defect, surface and auger recombination, these are briefly discussed at the end of this section. Photoluminescence measurements give information about the electronic properties, such as material bandgap. The high energy side of the emission spectum is attributed to thermal excitation of electrons to higher energy levels in the conduction band, and similarly for holes in the valence band. The shape of this tail can be modeled by a Boltzmann distribution for relatively high temperatures (T $>$ 100 K), as indicated in Eq. 5.4, where $I_h(E)$ is the intensity at photon energy E, k is the Boltzmann constant and T is the absolute temperature.

$$I_h(E) = Ae^{\frac{-E}{kT}} \tag{5.4}$$

Emission below the gap is possible due to thermal fluctuations in the lattice, and structural inhomogeneities. This low energy side of the peak can be modeled using the product of an Urbach edge [29] and a Boltzmann distribution, as shown in Eq. 5.5, where $I_l(E)$ is the intensity at photon

energy E, α_g is the 0 K absorption coefficient at the bandgap energy E_g and E_o is the Urbach parameter.

$$f(E) = \alpha_g e^{\frac{E-E_g}{E_o}} e^{-\frac{E-E_g}{kT}} \tag{5.5}$$

Light emission from LEDs is primarily a spontaneous emission process. From Eq. 5.1 we see that the rate of spontaneous emission between two levels is proportional to the product of the probability that the upper state is occupied and the probability the lower state is vacant. When a voltage is applied across an LED it causes a separation of quasi-Fermi levels equal to the applied voltage, which causes the occupation of a given level in the conduction band to increase and a decrease of the occupation of energy levels in the valence band, thus increasing the spontaneous emission rate.

Non-radiative recombination can be a significant, or even the dominant form of loss in a device depending on material quality and device design. There are three main types of non-radiative recombination; defect, surface and Auger recombination as shown in Fig. 5.1. Defect recombination is due to impurity atoms or defects in the crystal, which have mid-gap energy levels. In this case the electron can fall from the conduction band to the defect level and then recombine with a hole, thus depleting the conduction band without producing photons. Surface recombination is similar to defect recombination, except the mid-gap levels are surface states. Auger recombination requires two electrons in the conduction band. One electron falls to the valence band but the energy is used to push the other electron up to a higher energy level, thus depleting the conduction band without producing light.

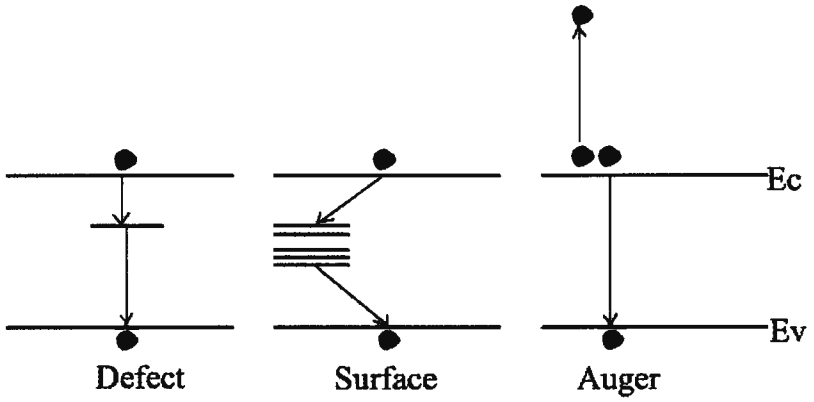

Figure 5.1: Possible non-radiative transitions in semiconductors.

5.2 Photoluminescence Measurements

As a semiconductor is cooled, it is expected that the bandgap will shift to higher energy. The shift in bandgap comes from a combination of a temperature-dependant dilation of the lattice and a temperature dependent electron-lattice interaction[30]. The temperature dependence can be described by the Varshni equation shown in 5.6, where α and β are constants, E_g is the bandgap energy at absolute temperature T and E_o is the bandgap energy at $T = 0$ K. For GaAs, $\alpha = 8.871x10^{-4}$ eV/K, $\beta = 572$ K and $E_0 = 1.5216$eV[31].

$$E_g(T) = E_o + \frac{\alpha T^2}{\beta + T} \tag{5.6}$$

Fig. 5.2 shows photoluminescence spectra for a series of temperatures from 8 K to room temperature (300 K) for $GaAs_{1-x}Bi_x$ sample r1965. The 532 nm green pump laser and collecting optics were focused on the area be-

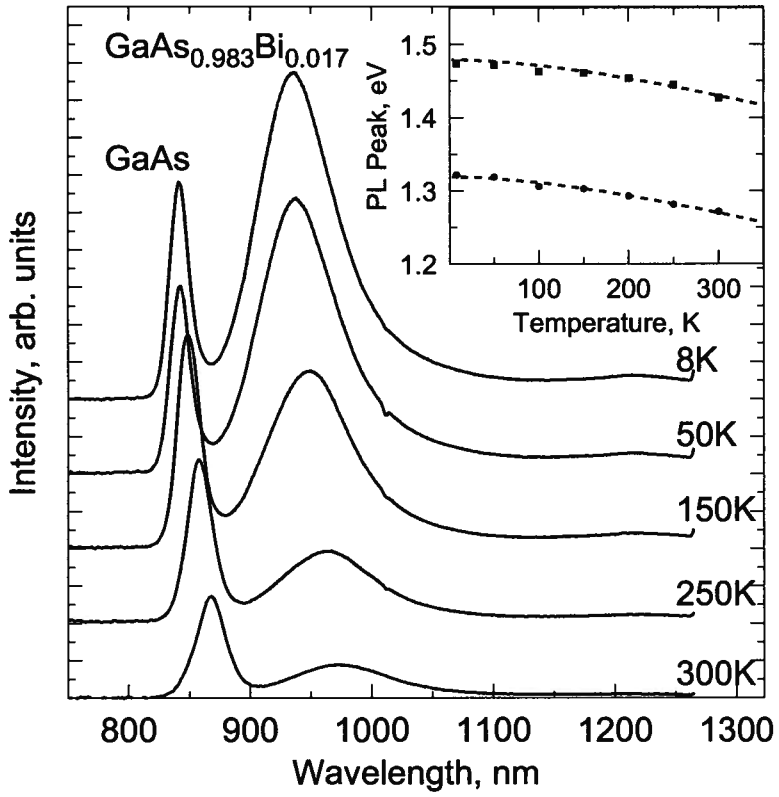

Figure 5.2: Photoluminescence spectra for $GaAs_{1-x}Bi_x$ LED structure r1965 over a temperature range of 8 K to 300 K. The inset shows the peak emission energies as a function of temperature for both the GaAs and $GaAs_{1-x}Bi_x$ peaks. A fit to the data using the Varshni equation is also shown (dashed line).

tween the metal dot contacts on the top of the sample. A clear peak was observed for both GaAs (870 nm) and $GaAs_{1-x}Bi_x$ (975 nm), along with a wide low energy tail which is attributed to shallow defect states in the bandgap. The $GaAs_{1-x}Bi_x$ peak emission wavelength at room temperature agrees with the expected shift in bandgap energy for 1.8 % bismuth incorporation, 0.16 eV[6]; this estimate for the bismuth content is consistent with a fit to the split off peak seen in the [004] XRD rocking curve which gave $x = 1.7 \pm 0.2\%$ for $GaAs_{1-x}Bi_x$. Both the GaAs and $GaAs_{1-x}Bi_x$ peaks blue shifted with decreasing temperature (inset of Fig. 5.2) and followed the Varshni equation[30]:

In the fit in the inset of Fig. 5.2, E_o for GaAs is 1.48 eV and $E_o = 1.32$ eV for $GaAs_{0.982}Bi_{0.018}$, with $\alpha = 0.36$ meV/K and $\beta = 356$ K in equation 5.6 for both fits. The change in E_o corresponds to 1.8% bismuth, based on 88 meV band gap reduction per percent bismuth incorporation[6]. Temperature dependent PL measurements were not made on other samples.

5.3 Electroluminescence Measurements

Electroluminescence (EL) measurements were made at room temperature unless otherwise stated. The light was collected from the periphery of the top metal dot, since the metal dot was opaque. EL spectra from $GaAs_{1-x}Bi_x$ light emitting diode r1965 are shown in Fig. 5.3 for forward bias current densities of 50 A/cm^2, 75 A/cm^2 and 100 A/cm^2.

Two clear peaks are seen: GaAs at 870 nm and $GaAs_{1-x}Bi_x$ at 987 nm, along with a low energy tail. With increasing current density a slight blue

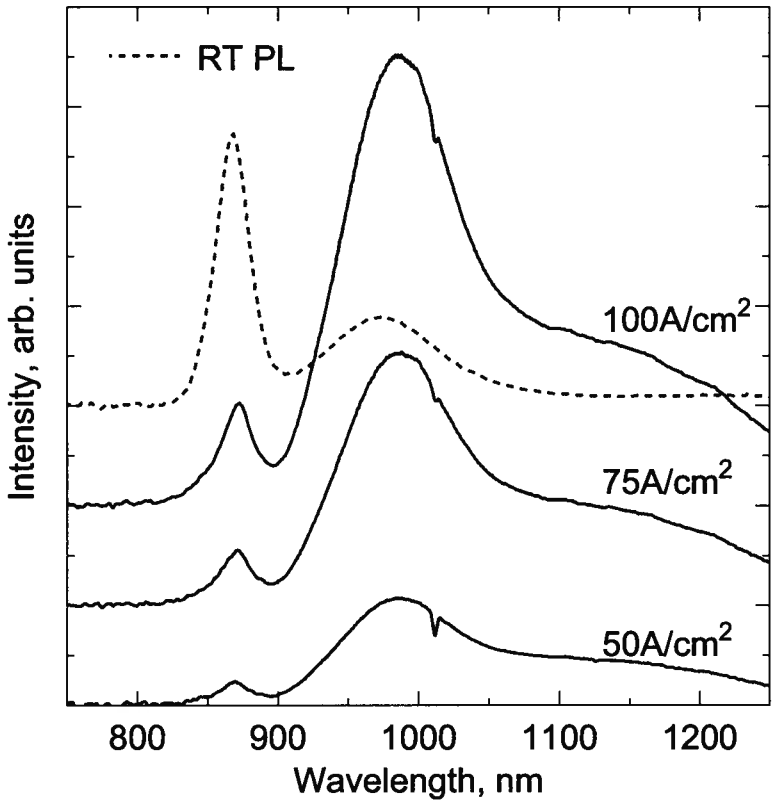

Figure 5.3: Electroluminescence spectra for a $GaAs_{1-x}Bi_x$ light emitting diode from sample r1965 for various injection current densities at 300 K. Room temperature photoluminescence is shown for comparison.

shift in the peak emission wavelength of the $GaAs_{1-x}Bi_x$ band to band peak was observed, attributed to a further separation of quasi-Fermi levels at higher pumping currents. The shape of the spectra did not change. The $GaAs_{1-x}Bi_x$ peak intensity was found to be superlinear with increasing current density, possibly due to defect recombination saturation, resulting in a higher fraction of additional carriers recombining radiatively.

The room temperature PL is also shown in Fig. 5.3 for comparison. PL peaks are blue shifted relative to the EL peaks and the low energy emission from the defect states is much stronger in the EL spectra. Both of these observations can be explained by the differences in the way carriers are injected for PL and EL. In the former case carriers are injected with energies larger than the bandgap, while in the latter case electrically injected carriers have energies close to the band edges and are thus restricted to low energy states. This results in an increasing tendency for recombination from higher energy states to occur in the case of PL.

Earlier LED samples performed more poorly than r1965 LEDs. Fig. 5.4 shows EL spectra from three $GaAs_{1-x}Bi_x$ LEDs at 100 A/cm^2 injection current. The black and red data are from two diodes (fabricated separately) from sample r1895, which contained about 1% bismuth. The blue data is from r1917, which contained 5.5% bismuth. EL intensity was very weak, compared to sample r1965 discussed above. All spectra show a peak at 870 nm, corresponding to GaAs and broadband emission at wavelengths exceeding 1000 nm, corresponding to emission from defects. Long wavelength emission intensities in Fig. 5.4, whether from defects or the $GaAs_{1-x}Bi_x$ layer, are all more than an order of magnitude smaller than the emission

from the $GaAs_{1-x}Bi_x$ layer from sample r1965 at the same injection current. The long wavelength emission from r1895 could not have come from the $GaAs_{1-x}Bi_x$ layer since XRD measurements from Fig. 2.5 showed the $GaAs_{1-x}Bi_x$ layer had $x = 0.01$. Based on 88 meV reduction of the bandgap per percent bismuth[6], the $GaAs_{1-x}Bi_x$ peak should have been at 930 nm. Sample r1917 was found by XRD measurements to have $x = 0.055$ in the $GaAs_{1-x}Bi_x$, which would put the expected $GaAs_{1-x}Bi_x$ peak at 1325 nm. Looking at the EL spectra in Fig. 5.4 it appears that the long wavelength emission (1000 nm to 1300 nm) from r1917 is composed of two broad peaks, the longer of which is at about 1300 nm, hence it is possible that some of this emission came from the $GaAs_{1-x}Bi_x$ layer. r1917 also had two growth interrupts, which is expected to have increased the amount of defects resulting in further loss in the EL from the $GaAs_{1-x}Bi_x$ layer.

Fig. 5.5 shows EL from the $In_xGa_{1-x}As$ LED (1929) with x=0.18 for current densities of 12 A/cm^2, 25 A/cm^2, 37 A/cm^2 and 62 A/cm^2. The spectra show a small GaAs peak at 870 nm and a large peak at 1025 nm from the $In_xGa_{1-x}As$ QWs. As observed with the $GaAs_{1-x}Bi_x$ LED, the peak of the $In_xGa_{1-x}As$ emission slightly blue shifted with increasing current density, due to further separation of the quasi-Fermi levels. No long wavelength tail from defects was observed in this sample. Unlike the $GaAs_{1-x}Bi_x$ LED, which showed super-linear light emission, emission form the $In_xGa_{1-x}As$ device was sub-linear, as can be seen in Fig. 5.5. This suggests that there was less non-radiative defect recombination to saturate. The integrated room temperature intensity of the $In_xGa_{1-x}As$ device was about 100× higher than for the r1965 $GaAs_{1-x}Bi_x$ device at the same current. Quantum wells are known to be

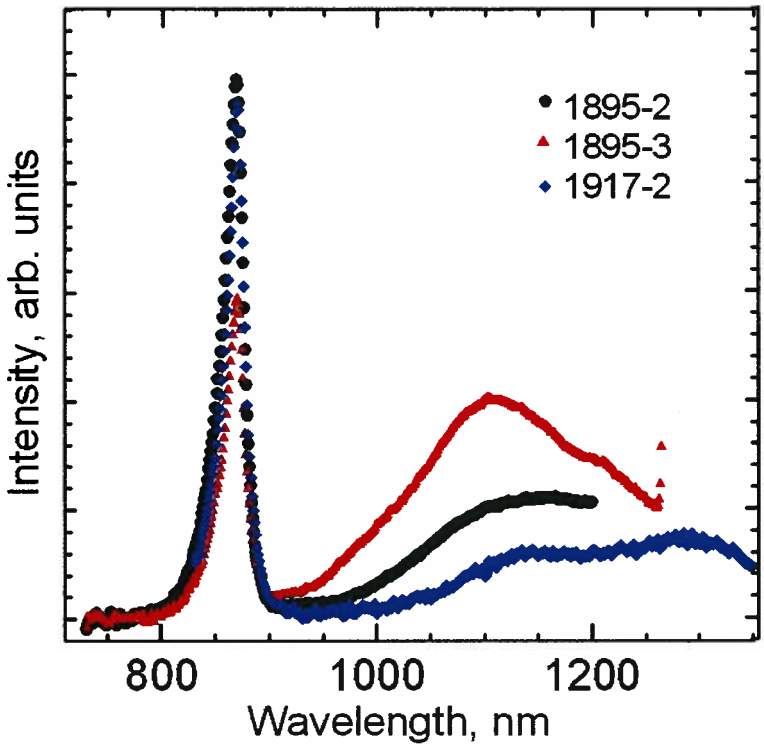

Figure 5.4: Room temperature electroluminescence spectra from three $GaAs_{1-x}Bi_x$ LEDs at 100 A/cm^2 injection current. The black and red spectra were fabricated from growth r1895 and contain 1% bismuth. The blue spectra (from r1917) contained 5.5% bismuth in the $GaAs_{1-x}Bi_x$ layer.

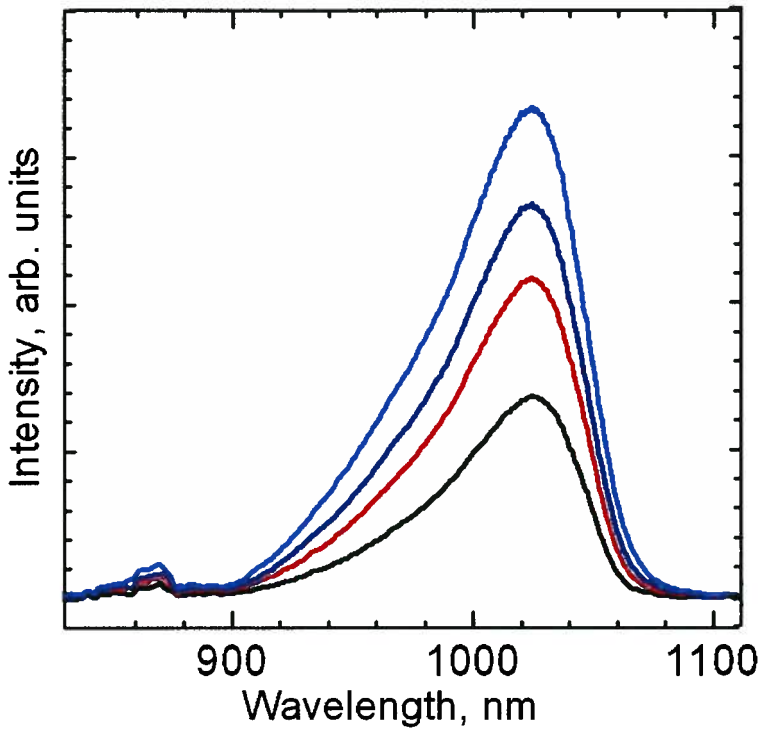

Figure 5.5: Room temperature electroluminescence spectra for an $In_xGa_{1-x}As$ light emitting diode for various injection current densities.

more efficient than bulk layers and it is expected that had the $GaAs_{1-x}Bi_x$ device also contained 3 similarly sized quantum wells that it would have been brighter than the existing $GaAs_{1-x}Bi_x$ design.

5.4 Temperature Dependent Electroluminescence

Fig. 5.6 shows the temperature dependence of the r1965 $GaAs_{1-x}Bi_x$ LED EL spectra at 50 A/cm^2 from 100 K to 300 K.

As the temperature decreased, a clear blue shift in the peak wavelength of the GaAs in agreement with PL results was observed. Both the emission from the $GaAs_{1-x}Bi_x$ peak and the longer wavelength shallow defect states increased with decreasing temperature. However, emission from the defect states also increased relative to the $GaAs_{1-x}Bi_x$ band to band peak. At 100 K the intensity of defect emission surpassed the emission of the $GaAs_{1-x}Bi_x$ band to band peak. In contrast to the PL measurements shown in Fig. 5.2, the intensity of the GaAs peak decreased as the device was cooled. This resulted from a greater carrier confinement in the smaller bandgap $GaAs_{1-x}Bi_x$ layer. No shift in peak wavelength of the $GaAs_{1-x}Bi_x$ emission was observed over this temperature range. This can be explained by two competing processes, the increase in the bandgap at lower temperature and the increased tendency for emission to come from lower energy states at lower temperatures. These two processes combined result in the observed temperature independent peak emission wavelength of the $GaAs_{1-x}Bi_x$ band to band electroluminescence. The temperature sensitivity of PL measurements can be

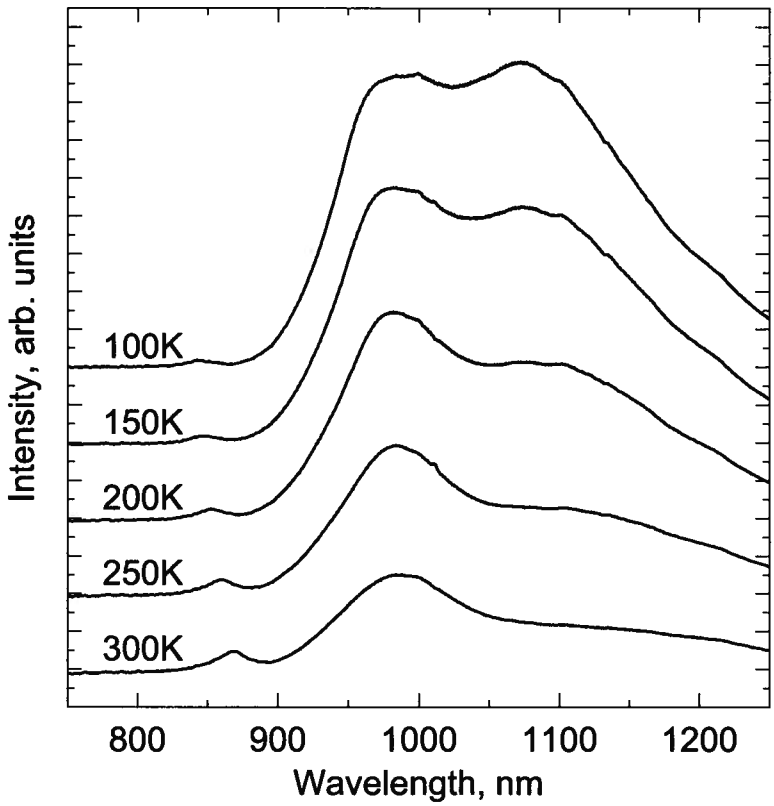

Figure 5.6: Electroluminescence spectra from GaAsBi LED r1965 at 50 A/cm^2 injection current density for temperatures ranging from 100 K to 300 K.

explained by the low density of states of the $GaAs_{1-x}Bi_x$ impurity like states in the bandgap. It is possible that as the temperature is lowered PL emission of these lower energy states does not increase because the electrons-hole pairs recombine before they have a chance to find the deeper impurity-like states.

Chapter 6

Conclusion

$GaAs_{1-x}Bi_x$ is an exciting new semiconductor with promising applications as a new infrared light source. The characteristics of the $GaAs_{1-x}Bi_x$ appear to be well matched to the requirements for optical coherence tomography.

We have developed a method for the growth and fabrication of $GaAs_{1-x}Bi_x$ light emitting diodes, based on a simple n-i-p structure containing one $GaAs_{1-x}Bi_x$ layer in the intrinsic region. n-i-p structures with up to 5.5% bismuth in the $GaAs_{1-x}Bi_x$ layer have been realized. Strong light emission was obtained from a sample containing 1.8% bismuth with emission centered at 987 nm. This $GaAs_{1-x}Bi_x$ emission peak was found to be independent of temperature over the temperature range 100 K to 300 K. The long wavelength emission did increase, which changed the shape of the spectra.

The temperature insensitivity of the $GaAs_{1-x}Bi_x$ electroluminescence can be explained by two competing processes; the increase in the bandgap with decreasing temperature and the tendency for emission to come from lower energy states as temperature is decreased. Photoluminescence measurements on the same device showed a temperature dependence of the $GaAs_{1-x}Bi_x$ band to band transition consistent with measurements by Francoeur[6]. Both the electroluminescence and photoluminescence spectra have large spectral widths which is a reflection of the impurity-like nature of the states associated

with bismuth incorporation. Difficulties incorporating bismuth into the n-i-p structure are an unresolved issue as well as the poor performance of many of the $GaAs_{1-x}Bi_x$ layers.

This demonstration of a $GaAs_{1-x}Bi_x$ based LED opens up a new class of materials for long wavelength semiconductor light sources with broad emission spectra.

6.1 Future Work

Much work must still be done to reliably grow $GaAs_{1-x}Bi_x$ LED structures with the desired amount of bismuth. The fact that many of the growths did not show strong luminescence from the $GaAs_{1-x}Bi_x$ layer also requires further investigation. GaAs n-i-p samples grown at different growth conditions were grown but have not yet been fabricated and characterized, this will have to be done to investigate whether the low temperature GaAs or the $GaAs_{1-x}Bi_x$ layer is the source of the impurity emission. New $GaAs_{1-x}Bi_x$ devices should also be grown and fabricated in attempt to obtain strong electroluminescence from a $GaAs_{1-x}Bi_x$ light emitting diode with 1.0 eV bandgap. This will show that $GaAs_{1-x}Bi_x$ devices can exceed the wavelength range of $In_xGa_{1-x}As$ devices. Improvements to this rudimentary test device could be made by: optimizing the thicknesses of the $GaAs_{1-x}Bi_x$ and undoped GaAs layers; optimizing contact design; the use of an AlGaAs double heterostructure design; and removing the growth interrupt.

Bibliography

[1] H. Föll. Christian-Albrechts-University of Kiel, http://www.tf.uni-kiel.de/matwis/amat/semi_en/kap_5/backbone/r5_1_4.html.

[2] X. Lu, D. Beaton, T. Tiedje, R. Lewis, M.B. Whitwick. Effect of MBE Growth Conditions on Bi Content of $GaAs_{1-x}Bi_x$. *Applied Physics Letters*, 92, 2008.

[3] M.J. Antonell, C.R. Abernathy, A. Sher, M. Berding, M. Van Schilfgaarde, A. Sanjuro K. Wong. Growth of Tl-Containing III-V Materials by Gas-Source Molecular Beam Epitaxy. *Journal of Crystal Growth*, 188:113–118, 1998.

[4] S. Tixier, M. Adamcyk, E.C. Young, J.H. Schmid, T. Tiedje. Surfactant enhanced growth of GaNAs and InGaNAs using bismuth. *Journal of Crystal Growth*, 251:449–454, 2003.

[5] K. Oe, H. Okamoto. New Semiconductor Alloy $GaAs_{1-x}Bi_x$ Grown by Metal Organic Vapor Phase Epitaxy. *Japanese Journal of Applied Physics Part 2*, 37:L1283–L1285, 1998.

[6] J. Yoshida, T. Kita, O. Wada, K. Oe. Temperature Dependence of GaAs1-xBix Band Gap Studied by Photoreflectance Spectroscopy. *Japanese Journal of Applied Physics Part 1*, 42:371, 2003.

[7] S. Francoeur, M.J. Seong, A. Mascarenhas, Sebastien Tixier, Martin Adamcyk, Thomas Tiedje. Band Gap of $GaAs_{1-x}Bi_x$, 0<3.6%. *Applied Physics Letters*, 82:3874–3876, 2003.

[8] S. Adachi. *Physical Properties of III-V Semiconductor Compounds.* Wiley, 1992.

[9] T. Tiedje, E.C. Young, A. Mascarenhas. Growth and Properties of the Dilute Bismide Semiconductor $GaAs_{1-x}Bi_x$ a Complementary Alloy to the Dilute Nitrides. *International Journal of Nanotechnology*, 5:963–983, 2008.

[10] 1.A. Janotti, S.H. Wei, S.B. Zhang. Theoretical study of the effects of isovalent coalloying of Bi and N in GaAs. *Physical Review B*, 65:115203, 2002.

[11] 1.W. Shan, W. Walukiewicz, J.W. Ager, E.E. Haller, J.F. Geisz, D.J. Friedman, J.M. Olson, S.R. Kurtz. Band Anticrossing in GaInNAs Alloys. *Physical Review Letters*, 82:1221, 1999.

[12] A. Mascarenhas, Y. Zhang, J. Veerley, M.J. Seong. Overcoming Limitations in Semiconductor Alloy Design. *Superlattices and Microstructures*, 29:395, 2001.

[13] L. Vegard. Die Konstitution der Mischkristalle und die Raumfullung der Atome. *Z. Physik*, 5:17, 1921.

[14] U. Tisch, E. Finkman, J. Salzman. The anomalous bandgap bowing in GaAsN. *Applied Physics Letters*, 81:463–465, 2002.

[15] E. Nodwell, M. Adamcyk, A. Ballestad, T. Tiedje, S. Tixier, S.E. Webster, E.C. Young, A. Moewes, E.Z. Kurmaev, T. van Buuren. Tight-Binding Model for the X-ray Absorption and Emission Spectra of Dilute GaNxAs1-x at the Nitrogen K edge. *Physical Review B*, 69:15520, 2004.

[16] K. Oe. Characteristics of Semiconductor Slloy GaAs1-xBix. *Japanese Journal of Applied Physics Part 1*, 41:2801–2806, 2002.

[17] D. Huang, E.A. Swanson, C.P. Lin, J.S Schuman, W.G. Stinson, W. Chang, M.R. Hee, T. Flotte, K. Gregory, C.A. Puliafito, J.G. Fujimoto. Optical Coherence Tomography. *Science*, 254:1178–1181, 1991.

[18] J.M. Schmitt. Optical Coherence Tomography (OCT): A Review. *IEEE Selected Topics in Quantum Electronics*, 5:1205, 1999.

[19] M.R. Pillai, S.S Kim, S.T. Ho, S.A. Barnett. Growth of $In_xGa_{1-x}As/GaAs$ heterostructures using Bi as a surfactant. *Journal of Vacuum Science and Technology B*, 18:1232–1236, 2000.

[20] E.C. Young, S. Tixier, T. Tiedje. Bismuth Surfactant Growth of the Dilute Nitride GaN_xAs_{1-x}. *Journal of Crystal Growth*, 279:316–320, 2005.

[21] L.A. Coldren, S.W. Corzine. *Diode Lasers and Photonic Integrated Circuits.* Wiley Series in Microwave and Optical Engineering, 1995.

[22] M. Balkanski, R.F. Wallis. *Semiconductor Physics and Applications.* Oxford, 2000.

[23] S.R. Johnson, C. Lavoie, T.Tiedje. Semiconductor Substrate Temperature Measurement by Diffuse Reflectance Spectroscopy in Molecular Beam Epitaxy. *Journal of Vacuum Science and Technology B*, 11:1007–1010, May 1993.

[24] R. Williams. *Modern GaAs Processing Methods.* Artech House, 1990.

[25] T.C. Shen, G.B. Gao, H. Morkoc. Recent Developments in Ohmic Contacts for III-V Compound Semiconductors. *Journal of Vacuum Science and Technology B*, 10:2113–2132, 1992.

[26] S.M. Sze. *Physics of Semiconductor Devices.* John Wiley and Sons, 1981.

[27] G. Stareev. Formation of Extremely Low Resistance Ti/Pt/Au Ohmic Contacts to p-GaAs. *Applied Physics Letters*, 62:2801–2803, 1993.

[28] A. Katz, C.R. Abernathy, S.J. Pearton. Pt/Au Homic Contacts to Ultrahigh Carbon-doped p-GaAs Formed by Rapid Thermal Processing. *Applied Physics Letters*, 56:1028–1030, 1990.

[29] W.D. Edwards, A.B. Torrens, W.A. Hartman. Specific Contact Resistance of Ohmic Contact to Gallium-Arsenide. *Solid-State Electronics*, 15:387, 1972.

[30] S.R. Johnson, T. Tiedje. Temperature Dependence of the Urbach Edge in GaAs. *Journal of Applied Physics*, 78:5609–5613, 1995.

[31] Y.P. Varshni. Temperature Dependence of the Energy Gap in Semiconductors. *Physics*, 334:149–154, 1967.

[32] M.D. Sturge. Optical Absorption of Gallium Arsenide between 0.6 and 2.75 eV. *Physical Review*, 127:768–773, 1962.